Physical properties of amorphous $Al_{90}Fe_5Ce_5$

1990 J. Phys.: Condens. Matter 2 4315

(http://iopscience.iop.org/0953-8984/2/19/001)

J. Phys.: Condens. Matter **2** (1990) 4315–4324. Printed in the UK

Physical properties of amorphous $Al_{90}Fe_5Ce_5$

R A Dunlap†, M H Yewondwossen†, V Srinivas†, I A Christie†, M E McHenry‡ and D J Lloyd§

† Department of Physics, Dalhousie University, Halifax, Nova Scotia, Canada B3H 3J5
‡ MST-6, Los Alamos National Laboratory, Los Alamos, NM 87545, USA
§ Kingston Research and Development Centre, Alcan International Limited, Kingston, Ontario, Canada K7L 4Z4

Received 2 August 1989, in final form 15 February 1990

Abstract. Amorphous $Al_{90}Fe_5Ce_5$, prepared by rapid solidification from the melt, shows unusual tensile strength. Here we have investigated various physical properties of this alloy. X-ray diffraction measurements indicate a mean interatomic spacing comparable to that in FCC aluminium. Thermal analysis studies show an onset of crystallisation at 543 K, corresponding to the precipitation of FCC Al in an amorphous matrix. A second exothermic reaction at 593 K corresponds to the crystallisation of the remaining amorphous component into FCC Al and an intermetallic phase, possible $Al(Ce, Fe)_3$. The electrical resistivity is well described by the Ziman–Faber theory with a Debye temperature of ~200 K. Magnetic susceptibility shows the alloy to be paramagnetic and to exhibit combined Curie and Pauli behaviour. ^{57}Fe Mössbauer effect measurements show the short range ordering of this alloy to be similar to that found in transition metal–metalloid glasses.

1. Introduction

Transition metal glasses have been studied extensively during the past decade and have found a number of applications based on their unusual mechanical and magnetic properties. The possibility of preparing amorphous alloys based on aluminium is attractive for mechanical applications, not only because of the possibility of high strengths, but because of the added feature of low density. Mixed phase Al-based alloys containing an amorphous component were first reported in binary Al–X (X = Cr, Ni, Cu, Pd, Si and Ge), see Inoue *et al* (1988a) and references therein. Single phase Al-based glasses have subsequently been reported in Al–Fe–B, Al–Co–B (Inoue *et al* 1981), Al–Fe–Si and Al–Fe–Ge (Suzuki *et al* 1983). The interest in rapidly solidified Al-based alloys, which began in 1984 with the discovery of Al–Mn quasicrystals (Shechtman *et al* 1984), and the subsequent search for new quasicrystalline materials has revealed numerous other Al-based systems which can be prepared as single phase amorphous alloys (see e.g. Dunlap and Dini 1986). While these amorphous Al-based alloys showed poor ductility and low tensile strengths, recently developed rare-earth-containing Al-based glasses have shown exceptional tensile strengths (Inoue *et al* 1988b, c, d, He *et al* 1988) and have opened up the possibiliity of commercial applications for these low-density, high-strength materials. In the present work we report on the first characterisation of the physical properties of one of these alloys, $Al_{90}Fe_5Ce_5$. We report on x-ray diffraction, thermal analysis, electrical resistivity, magnetic susceptibility and Mössbauer effect studies.

0953-8984/90/194315 + 10 $03.50

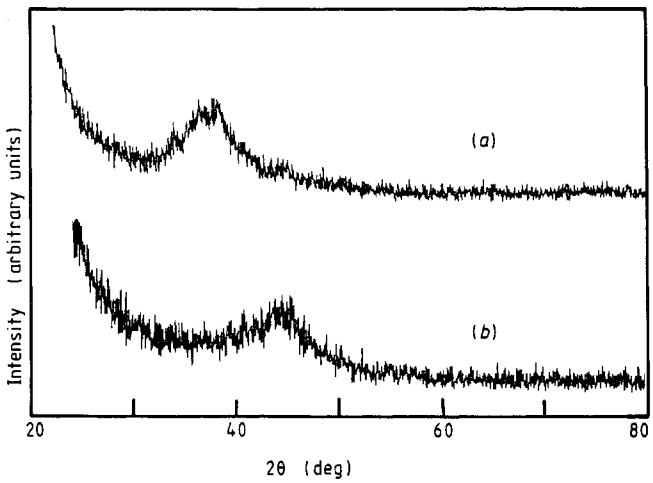

Figure 1. Cu Kα x-ray diffraction patterns of amorphous alloys (*a*) $Al_{90}Fe_5Ce_5$ and (*b*) $Al_{50}Mn_{20}Si_{30}$.

2. Experimental methods

$Al_{90}Fe_5Ce_5$ ribbons were prepared in the fully amorphous state by rapid quenching onto the surface of a single copper roller.

Room temperature x-ray diffraction studies were performed using Cu Kα radiation on a Siemens D500 scanning powder diffractometer.

Differential thermal analysis (DTA) measurements were made under an argon atmosphere on a Fisher 260F thermal analyser. The heating rate for all measurements was 20 K min^{-1}.

Electrical resistivity studies were made between 4 K and 300 K using a conventional 4-point DC method.

Magnetic susceptibility measurements were made between 4 K and 300 K in an applied field of 10 kOe using a SHE SQUID (superconducting quantum interference device) magnetometer.

^{57}Fe Mössbauer measurements were made at room temperature using a Pd^{57}Co source and a Wissel System II Mössbauer spectrometer. The intrinsic linewidth of the spectrometer for a thin α-Fe absorber was found to be 0.228 mm s^{-1} (full width half maximum).

3. Results and discussion

3.1. X-ray diffraction measurements

The room temperature Cu Kα x-ray diffraction pattern of $Al_{90}Fe_5Ce_5$ is illustrated in figure 1. For comparison, the diffraction pattern of amorphous $Al_{50}Mn_{20}Si_{30}$ (Dunlap *et al* 1989) is illustrated, as well. The location of the major diffuse peak in these two alloys gives an average interatomic distance for a dense random structure of $d = \sqrt{6}\lambda/(4 \sin \theta)$ or 2.90 Å for Al–Fe–Ce and 2.40 Å for Al–Mn–Si. The anomalously large value for Al–Fe–Ce, presumably, results in the large concentration of Al in this alloy and corresponds well to the interatomic bond length of 2.863 Å in FCC aluminium.

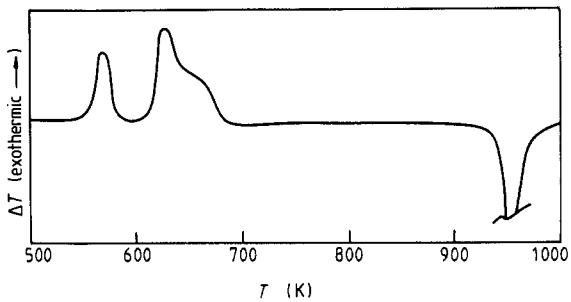

Figure 2. Differential thermal analysis scan of amorphous $Al_{90}Fe_5Ce_5$ obtained using a heating rate of 20 K min^{-1}.

These results are in general agreement with those reported for similar alloys by He *et al* (1988).

3.2. Thermal analysis measurements

A differential thermal analysis (DTA) scan of $Al_{90}Fe_5Ce_5$ is illustrated in figure 2. This measurement shows two exothermic peaks with onsets at 543 K and 593 K, and a large endothermic peak with an onset of 923 K. A sample heated to 570 K at 20 K min^{-1}, followed by water quenching, shows an x-ray diffraction pattern indicating the presence of a remaining amorphous phase plus FCC Al. This indicates that the lower temperature exotherm corresponds to the precipitation of aluminium in the amorphous matrix. An x-ray diffraction pattern of a sample heated to 650 K shows that the final crystallisation products are FCC aluminium and an intermetallic phase which can be indexed satisfactorily to the $AlCe_3$ structure with a slightly altered lattice parameter. It is possible, therefore, that this phase is $Al(Ce, Fe)_3$. The large endotherm at higher temperature results from the melting of the FCC Al component.

3.3. Electrical resistivity measurements

The normalised resistivity, $\rho(T)/\rho(300)$, measured as a function of temperature for amorphous $Al_{90}Fe_5Ce_5$ is illustrated in figure 3. The absolute value of the room temperature resistivity has been found to be $80 \pm 10\ \mu\Omega$ cm. This value is consistent with the positive room temperature coefficient of resistivity in the context of the correlation between $\rho(300)$ and $\partial\rho(T)/\partial T|_{300}$ described by Mooji (1973). The temperature dependence of $\rho(T)$ in this alloy is best described on the basis of the Ziman–Faber model (Ziman 1961, Faber and Ziman 1965) in the following way.

Faber and Ziman (1965) have described a resistivity for a disordered material which is proportional to the structure factor, $S(K)$, of the material. Meisel and Cote (1977) have expanded the structure factor as

$$S(K) = S_0(K) + S_1(K) + S_2(K) + \ldots \tag{1}$$

where $S_i(K)$ is the ith phonon scattering term. They have evaluated the low-temperature dependence of the total $S(K)$ which, in terms of a positive parameter a, is

$$S(K) = 1 + aT^2 \tag{2}$$

for $T < \theta_D/2$, where θ_D is the Debye temperature. For $T > \theta_D/2$ Meisel and Cote (1977) have determined $S(K)$ according to the Ziman–Faber theory as

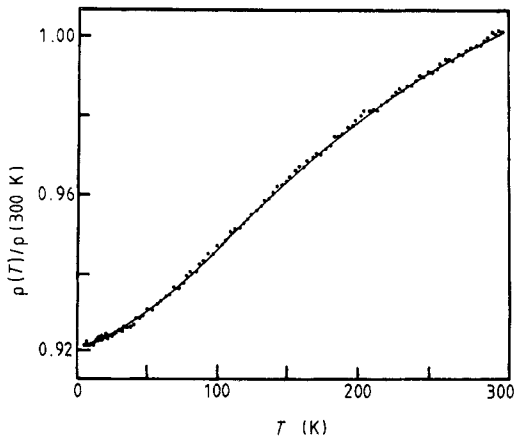

Figure 3. Normalised resistivity of amorphous $Al_{90}Fe_5Ce_5$ as a function of temperature. The solid line represents a computer fit to the data as described in the text.

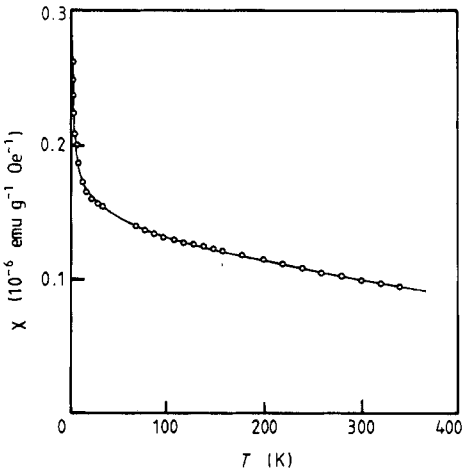

Figure 4. Magnetic susceptibility of amorphous $Al_{90}Fe_5Ce_5$ measured as a function of temperature in an applied external field of 10 kOe. The solid line represents a computer fit to the data as described in the text.

$$S(K) = bT. \tag{3}$$

Based on equations (2) and (3), the data illustrated in figure 3 are well described by expressions of the form

$$\left.\begin{aligned} \rho(T)/\rho(300) &= a_1 + a_2T^2 \qquad T < \theta_D/2 \\ \rho(T)/\rho(300) &= b_1 + b_2T \qquad T > \theta_D/2 \end{aligned}\right\} \tag{4}$$

with $a_1 = 4.3 \times 10^{-1}$, $a_2 = 1.23 \times 10^{-6}\,K^{-2}$, $b_1 = 4.3 \times 10^{-1}$, $b_2 = 1.24 \times 10^{-4}\,K^{-1}$ and $\theta_D \approx 200$ K. These observations indicate that the resistivity in the material is well described on the basis of scattering due to structural disorder. This alloy is only very weakly paramagnetic (see section 3.4 below); a resistivity based entirely on its structural properties is consistent with our *a priori* expectations. The Debye temperature is consistent with that reported previously for metastable Al-based quasicrystals (Berger *et al* 1988).

3.4. Magnetic susceptibility measurements

The magnetic susceptibility of amorphous $Al_{90}Fe_5Ce_5$, measured in an applied DC magnetic field of 10 kOe is illustrated in figure 4. The susceptibilities which are observed in this material are very small and, as a result, the freezing of spins due to paramagnetic oxygen present in the susceptometer interferes with measurements in the neighbourhood of 55 K and is responsible for the lack of data in this region. The characteristics observed in figure 4, i.e. a Curie-like behaviour at low temperatures and a linearly decreasing susceptibility at higher temperatures, has been observed previously in icosahedral aluminium early–late transition metal alloys by Srinivas *et al* (1989). This behaviour has been described as a mixture of Curie-like behaviour due to a localised Fe moment and a Pauli contribution from the conduction band and has been expressed as

$$\chi(T) = A + BT + C/(T - \theta). \tag{5}$$

Here θ is the paramagnetic Curie temperature and C is related to the localised moment, μ, as

Table 1. Parameters obtained from magnetic susceptibility data for amorphous Al–Fe–Ce and a comparison with icosahedral Al–Ta–Fe and Al–Mo–Fe.

Alloy	A (emu g^{-1} Oe^{-1})	B (emu g^{-1} Oe^{-1} K^{-1})	θ (K)	C (emu K g^{-1} Oe^{-1})	μ (μ_B)	Reference
		Amorphous phase				
$Al_{90}Fe_5Ce_5$	1.47×10^{-7}	-1.46×10^{-10}	1.2	8.0×10^{-8}	0.02	†
		Quasicrystalline phase				
$Al_{70}Ta_{10}Fe_{20}$	9.29×10^{-5}	-4.32×10^{-8}	2.6	1.13×10^{-4}	0.48	‡
$Al_{80}Mo_9Fe_{11}$	1.0×10^{-5}	-5.15×10^{-9}	3.9	1.4×10^{-5}	0.19	‡

† This work.
‡ Srinivas *et al* (1989).

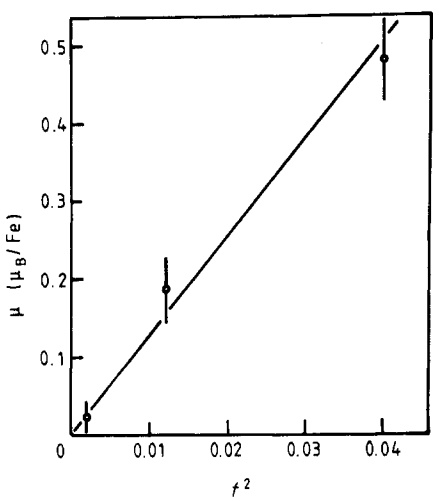

Figure 5. Relationship between the Fe magnetic moment, μ, and the square of the Fe content, f^2. The line is constrained to pass through the origin.

$$C = \mu_B^2 \mu^2 / 3k_B \tag{6}$$

where μ_B is the Bohr magneton and k_B is Boltzman's constant. Results of a least squares fit to the data of figure 4 for equations (5) and (6) are given in table 1. For comparison, the results of the same analysis to the susceptibility of icosahedral Al–Ta–Fe and Al–Mo–Fe, as reported by Srinivas *et al* (1989) are included. Clearly, these data illustrate that all aspects of the magnetic properties of amorphous $Al_{90}Fe_5Ce_5$ are weaker than those of the icosahedral alloys given in the table. Dunlap *et al* (1989) and Hauser *et al* (1986) have shown that there are relatively small differences between the magnetic properties of amorphous and icosahedral Al–Mn–Si alloys of similar composition. As well, Hauser *et al* (1986) have shown that, at least in some icosahedral alloy systems, the formation of an Mn moment can be described in terms of the probability of Mn–Mn nearest neighbour pair occurrence and hence μ is linear in f^2 (f = fraction of magnetic species). Dunlap *et al* (1990a) have shown that a similar description can be applied to Fe moment formation in some quasicrystals as well. Figure 5 illustrates that the data presented in table 1 are reasonably well described by a $\mu \propto f^2$ behaviour. This suggests that d-band overlap is, at least in part, responsible for magnetic moment formation. Although, as pointed out by Dunlap *et al* (1990a) for icosahedral alloys, the degree of local disorder is an important consideration in analysing the magnetic properties in these materials. Further discussion along these lines will be given in the section on Mössbauer spectral analysis below.

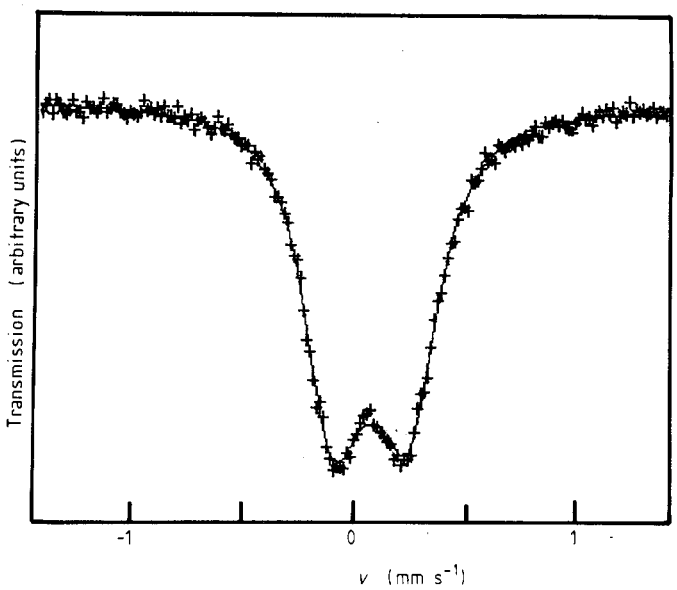

Figure 6. The room temperature ^{57}Fe Mössbauer effect spectrum of amorphous $Al_{90}Fe_5Ce_5$. The solid line is a least square fit using the model of LeCaer and Dubois (1979).

Table 2. Results of a fiting to two-Lorentzian lines. Δ is the quadrupole splitting, γ is the isomer shift relative to α-Fe at room temperature, Γ_1 is the width (FWHM) of the ith line (i = 1 is the more negative velocity component), A_i is the amplitude of the ith line. Velocities are in mm s^{-1} with an accuracy of ± 0.005 mm s^{-1}.

	Analysis method			
Parameter	Two Lorentzian	Shell model	LeCaer–Dubois method	Eibschultz method
$\bar{\Delta}$	0.309	0.332	0.324	0.322
$\bar{\delta}$	+0.166	—	—	+0.169
Γ_1	0.299	—	—	—
Γ_2	0.322	—	—	—
A_1/A_2	0.89	—	—	—
δ_0	—	+0.167	+0.166	—
σ	—	0.242	—	—
α	—	0.013	0.017	—
n	—	1.32	—	—
ξ_1	—	—	—	0.186
ξ_2	—	—	—	0.164
$2\langle\Delta\delta\Delta u\rangle$	—	—	—	+0.00098
$\langle(\Delta\delta)^2\rangle + \langle(\Delta u)^2\rangle$	—	—	—	0.032

3.5. Mössbauer effect measurements

A room temperature ^{57}Fe Mössbauer effect spectrum of amorphous $Al_{90}Fe_5Ce_5$ is illustrated in figure 6. In order to obtain average parameters, we have fitted this spectrum to the two broadened Lorentzian lines. Results of this fit are given in table 2. The mean quadrupole splitting is slightly smaller than that observed in most other Al-based amorphous alloys (e.g. Eibschutz *et al* 1986). The anomalous linewidths are

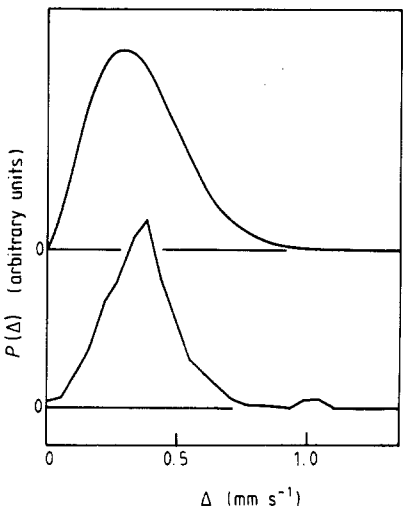

Figure 7. Quadrupole splitting distributions for amorphous $Al_{90}Fe_5Ce_5$ obtained from (*a*) the shell model and (*b*) the LeCaer–Dubois method.

characteristic of disordered materials (i.e. amorphous and quasicrystalline materials) and result from a distribution of local Fe environments. While some controversy has surrounded the fitting of Mössbauer spectra of icosahedral alloys (e.g. Dunlap *et al* 1988b), the situation in amorphous alloys is more clearly defined. Several models have been proposed for dealing with such distributions in amorphous alloys. Here we have applied several analysis methods which have been found useful in the past in extracting information from the Mössbauer spectra of amorphous alloys. For all cases in which this spectrum was analysed on the basis of a distribution of quadrupole splittings, Δ, the intrinsic line width of the component spectra was taken to be the resolution of the spectrometer for ^{57}Fe: 0.228 mm s^{-1} (FWHM).

Shell model analysis. The shell model has been proposed for the analysis of Mössbauer spectra of paramagnetic amorphous alloys by Czjzek (1982). This model expands the probability distribution for the quadrupole splitting, $P(\Delta)$, as (Eibschutz *et al* 1986)

$$P(\Delta) \propto (\Delta/\sigma)^n \exp(-\Delta^2/2\sigma^2) \tag{7}$$

where n and σ are fitted parameters. To account for any spectral asymmetry, the isomer shift δ is correlated to the quadrupole splitting, Δ, as a power series of the form

$$\delta(\Delta) = \delta_0 + \alpha\Delta + \beta\Delta^2 + \ldots . \tag{8}$$

Typically, it is found that terms to order Δ are sufficient to describe the spectra of these types of materials. For the alloy studied here, amorphous $Al_{90}Fe_5Ce_5$, this analysis yields the parameters given in table 2. The mean quadrupole splitting for the shell model is given by Lawther *et al* (1989) in terms of the fitted parameters as

$$\bar{\Delta} = \sqrt{2}\sigma\Gamma[(n+2)/2]/\Gamma[(n+1)/2] \tag{9}$$

where $\Gamma(x)$ is the Riemann gamma function. The quadrupole splitting distribution obtained from this method is illustrated in figure 7. The value of $\bar{\Delta}$ is slightly larger but is consistent with Δ found from the two-Lorentzian fit. The value of δ_0 is essentially the same as δ from the two-Lorentzian fit, as is expected for spectra with small values of α (i.e. little asymmetry). The value of n is small compared with the typical values of 2.0–2.5, as reported for Fe Mössbauer spectra of icosahedral Al-based alloys. As suggested

by Srinivas *et al* (1990), values of n near unity are characteristic of alloys with considerable disorder and are typical of amorphous materials.

LeCaer–Dubois analysis. LeCaer and Dubois (1979) have suggested an analysis of $P(\Delta)$ on the basis of an expansion in terms of discrete values. The form of $\delta(\Delta)$ in equation (8) is used. Fitted parameters are given in table 2 and the resulting $P(\Delta)$ is shown in figure 7. Values of δ_0, $\bar{\Delta}$ and α are consistent with those extracted from the shell model. In particular, it is important to note that for this alloy $P(\Delta \rightarrow 0) \rightarrow 0$ for the LeCaer–Dubois method. This is a condition of the functional form of the shell model, as can be seen in equation (7). Agreement of this type for these two fitting methods is not typically seen for icosahedral Al-based alloys as demonstrated by Dunlap *et al* (1990b).

Eibschutz analysis. Eibschutz and co-workers (e.g. Eibschutz 1983) have suggested a method of analysing hyperfine field distributed spectra of disordered (including amorphous) ferromagnets on the basis of Gaussian distributed Lorentzian line shapes for the purpose of obtaining information concerning correlations between splitting parameters and the isomer shift. Dunlap *et al* (1988a) have presented an analysis of Mössbauer spectra of amorphous paramagnets based on this scheme. The spectral data, $I(v)$, are fitted to two Gaussian distributions of Lorentzian shaped lines of the form

$$I(v) = I_0 - \sum_{i=1}^{2} I_i \int_{-\infty}^{\infty} P_i(v')L(v, v')\,\mathrm{d}v \tag{10}$$

where I_0 is the background, the I_i are fitted intensity parameters, L is a Lorentzian of the intrinsic line width centred at v', and P_i is a Gaussian distribution centred on the ith spectral line ($i = 1, 2$ for paramagnetic split spectra), of the form

$$P_i(v') = (1/\sqrt{2\pi}\xi_i)\exp[-(v' - v_i)^2/2\xi_i^2] \tag{11}$$

v is the velocity and, in equation (10), the integration is, for practical purposes, over the velocity range of the spectrum. In equation (11) v_i is the mean velocity position of the ith spectral line and is related to the mean isomer shift, $\bar{\delta}$, and quadrupole splitting $\bar{\Delta}$ as

$$v_1 = \bar{\delta} - \bar{u} \tag{12}$$

$$v_2 = \bar{\delta} + \bar{u} \tag{13}$$

where $i = 1$ corresponds to the more negative spectral line and the half splitting is defined in (12) and (13) to be

$$\bar{u} = \bar{\Delta}/a. \tag{14}$$

The full width at half maximum of the Gaussian distribution of the ith component, σ_i, is related to ξ_i in equation (11) by

$$\sigma_i = (8 \ln 2)^{1/2}\xi_i. \tag{15}$$

In the above, the fitted parameters are I_i, ξ_i and v_i.

In the case of quadrupole split spectra, there is an insufficient number of coupled equations to yield mean isomer shift and quadrupole distributions, $\langle \Delta\delta \rangle$ and $\langle \Delta\mu \rangle$, respectively. However, it can be shown (Dunlap *et al* 1988a) that fitted values of σ_i are sufficient to extract coupled terms of the form

$$\langle (\Delta\delta)^2 \rangle + \langle (\Delta u)^2 \rangle = (16 \ln 2)^{-1}(\sigma_2^2 + \sigma_1^2) \tag{16}$$

$$\langle \Delta\delta \Delta u \rangle = (32 \ln 2)^{-1}(\sigma_2^2 - \sigma_1). \tag{17}$$

The results of this analysis are given in table 2. The value for $\bar{\Delta}$ is essentially the same as those from the shell model and the method of LeCaer and Dubois, and is slightly larger than that from the two-Lorentzian fit. The mean isomer shift, $\bar{\delta}$, is the same as that obtained from the two-Lorentzian fits and the value of δ_0 from fits using either method involving a distribution of Δ. Values of $2\langle\Delta\delta\Delta u\rangle$ and $\langle(\Delta\delta)^2\rangle + \langle(\Delta u)^2\rangle$ have little direct significance, but allow for a comparison of microscopic environments with other disordered materials. Although there is not a significant source of data for comparison, Dunlap *et al* (1988a) have reported a similar analysis for amorphous $Cr_{72-x}Fe_xC_{17}Si_8Al_3$ alloys. For $x = 5 \ldots 40$, values ranged between -0.008 and $-0.0003\ \mathrm{mm^2\,s^{-2}}$ for $2\langle\Delta\delta\Delta u\rangle$ and between 0.018 and $0.044\ \mathrm{mm^2\,s^{-2}}$ for $\langle(\Delta\delta)^2\rangle + \langle(\Delta u)^2\rangle$. The values shown in table 2 for the present analysis are certainly consistent with the previous values for $\langle(\Delta\delta)^2\rangle + \langle(\Delta u)^2\rangle$ and the magnitude (although not the sign) of $2\langle\Delta\delta\Delta u\rangle$. These results indicate that the extent of the distribution of isomer shifts and of quadrupole splittings, as well as the magnitude of the correlation between these distributions in amorphous $Al_{90}Fe_5Ce_5$, is comparable to that observed in other amorphous paramagnets. The sign of the correlation between hyperfine parameters as extracted from ^{57}Fe Mössbauer measurements in disordered materials is, by no means, universal and differences between even closely related alloys are not uncommon.

4. Conclusions

We can draw the following conclusions from the data presented here:

(i) The mean interatomic spacing in amorphous $Al_{90}Fe_5Ce_5$ is comparable to that in FCC aluminium.

(ii) This alloy crystallises in two stages: first by the precipitation of FCC Al at 543 K and then by the formation of additional FCC Al and a second intermetallic phase at 593 K. These crystallisation temperatures are sufficiently low as to make commercial utilisation of this high tensile strength material in the form of a compacted solid difficult.

(iii) The electrical resistivity is well described in terms of the Ziman–Faber model for disordered materials with a Debye temperature near 200 K. The applicability of this model indicates a scattering mechanism based on structural disorder. The resistivity, $80\ \mu\Omega$ cm, is consistent, on the basis of the Mooji correlation, with the positive temperature coefficient of resistivity at room temperature.

(iv) This material is weakly paramagnetic and exhibits combined Curie-like behaviour (with a localised Fe moment of $0.02\ \mu_B$ at low temperature) and Pauli paramagnetism at higher temperatures. This same behaviour has been seen previously in some Al-based quasicrystals. The magnitude of the Fe moment in this alloy and in other disordered Al–Fe–transition metal alloys is consistent with moment formation as a result of d-band overlap.

(v) ^{57}Fe Mössbauer spectroscopy indicates a distribution of quadrupole splittings resulting from a distribution of local Fe environments. The shape of the distribution in Δ is suitably described by the shell model. An analysis based on the method of Eibschutz *et al* (1983), also indicates that the distribution of quadrupole splitting and isomer shift values, as well as the magnitude of the correlation between these distributions, is comparable to that seen in paramagnetic transition-metal-based amorphous alloys.

Acknowledgments

This work was supported by grants from the Natural Sciences and Engineering Research Council of Canada in conjunction with Alcan International Limited.

References

Berger C, Lasjaunias J C, Thoulence J L, Pavuna D and Germi P 1988 *Phys. Rev.* B **37** 6525
Czjzek G 1982 *Phys. Rev.* B **25** 4908
Dunlap R A and Dini K 1986 *J. Mater. Res.* **1** 415
Dunlap R A, Lawther D W, Hargraves P and Sinclair P 1988a *J. Phys. F: Met. Phys.* **18** 2479
Dunlap R A, Lawther D W and Lloyd D J 1988b *Phys. Rev.* B **38** 3649
Dunlap R A, McHenry M E, Srinivas V, Bahadur D and O'Handley R C 1989 *Phys. Rev.* B **39** 4808
Dunlap R A, O'Handley R C, McHenry M E and Srinivas V 1990a *Symmetry* at press
Dunlap R A, Srinivas V, Lloyd D J and Jha S 1990b *Hyperfine Interact.* at press
Eibschutz M, Chen H S and Hauser J J 1986 *Phys. Rev. Lett.* **56** 169
Eibschutz M, Lines M E and Chen H S 1983 *Phys. Rev.* B **28** 425
Faber T E and Ziman J M 1965 *Phil. Mag.* **11** 153
Hauser J J, Chen H S and Waszczak J V 1986 *Phys. Rev.* B **33** 3577
He Y, Poon S J and Shiflet G J 1988 *Science* **241** 1640
Inoue A, Kitamura and Masumoto T 1981 *J. Mater. Sci.* **16** 1895
Inoue A, Ohtera K, Kita K and Masumoto T 1988a *Japan. J. Appl. Phys.* **27** L1796
Inoue A, Ohtera K and Masumoto T 1988b *Japan. J. Appl. Phys.* **27** L736
Inoue A, Ohtera K, Tsau A P, Kimura H and Masumoto T 1988c *Japan. J. Appl. Phys.* **27** L1579
Inoue A, Ohtera K, Tsai A P and Masumoto T 1988d *Japan. J. Appl. Phys.* **27** L479
Lawther D W, Dunlap R A, Lloyd D J and Jha S 1990 *Hyperfine Interact.* at press
LeCaer G and Dubois M 1979 *J. Phys. E: Sci. Instrum.* **12** 1083
Meisel L V and Cote P J 1977 *Phys. Rev.* B **16** 2978
Mooji J H 1973 *Phys. Status Solidi* a **17** 521
Shechtman D, Gratias D, Belch I and Chan J W 1984 *Phys. Rev. Lett.* **54** 1951
Srinivas V, Dunlap R A, Bahadur D and Dunlap E 1990 *Phil. Mag.* B **61** 177
Srinivas V, McHenry M E and Dunlap R A 1989 *Phys. Rev.* B **40** 9590
Suzuki R O, Komatsu Y, Kobayashi K E and Shingu P H 1983 *J. Mater. Sci.* **18** 1195
Ziman J M 1961 *Phil. Mag.* **6** 1014